

Research



Cite this article: Kellom M, Pagliara S, Richards TA, Santoro AE. 2022 Exaggerated trans-membrane charge of ammonium transporters in nutrient-poor marine environments. *Open Biol.* **12**: 220041. <https://doi.org/10.1098/rsob.220041>

Received: 9 February 2022

Accepted: 13 June 2022

Subject Area:

microbiology/molecular biology/bioinformatics

Keywords:

competition, SAR11, SAR86, Thermoproteota, Thaumarchaea, membrane transport

Authors for correspondence:

Matthew Kellom

e-mail: mkellom@lbl.gov

Alyson E. Santoro

e-mail: asantoro@ucsb.edu

[†]Present address: DOE Joint Genome Institute, Lawrence Berkeley National Laboratory, Berkeley, CA, USA.

Electronic supplementary material is available online at <https://doi.org/10.6084/m9.figshare.c.6070031>.

Exaggerated trans-membrane charge of ammonium transporters in nutrient-poor marine environments

Matthew Kellom^{1,†}, Stefano Pagliara², Thomas A. Richards³ and Alyson E. Santoro¹

¹Department of Ecology, Evolution, and Marine Biology, University of California, Santa Barbara, CA, USA

²Living Systems Institute and Biosciences, University of Exeter, Exeter, Devon EX4 4QD, UK

³Department of Zoology, University of Oxford, 11a Mansfield Road, Oxford OX1 3SZ, UK

MK, 0000-0002-8310-7078; SP, 0000-0001-9796-1956; TAR, 0000-0002-9692-0973; AES, 0000-0003-2503-8219

Transporter proteins are a vital interface between cells and their environment. In nutrient-limited environments, microbes with transporters that are effective at bringing substrates into their cells will gain a competitive advantage over variants with reduced transport function. Microbial ammonium transporters (Amt) bring ammonium into the cytoplasm from the surrounding periplasm space, but diagnosing Amt adaptations to low nutrient environments solely from sequence data has been elusive. Here, we report altered Amt sequence amino acid distribution from deep marine samples compared to variants sampled from shallow water in two important microbial lineages of the marine water column community—Marine Group I Archaea (Thermoproteota) and the uncultivated gammaproteobacterial lineage SAR86. This pattern indicates an evolutionary pressure towards an increasing dipole in Amt for these clades in deep ocean environments and is predicted to generate stronger electric fields facilitating ammonium acquisition. This pattern of increasing dipole charge with depth was not observed in lineages capable of accessing alternative nitrogen sources, including the abundant alphaproteobacterial clade SAR11. We speculate that competition for ammonium in the deep ocean drives transporter sequence evolution. The low concentration of ammonium in the deep ocean is therefore likely due to rapid uptake by Amts concurrent with decreasing nutrient flux.

1. Introduction

Competition for resources is a fundamental driver of evolution [1–3]. Microbes living in low-nutrient environments, such as the open ocean, are under pressure to outcompete their neighbours, vying for limited resources [1,2,4]. Proteins that allow the acquisition and utilization of substrates at low concentrations may thus be under strong selection pressure. However, diagnosing quantitative variation in substrate affinity from sequence data alone can be challenging [5], inhibiting our ability to interpret competition between uncultivated microbes from metagenomic data.

Membrane-bound transporters are protein complexes that facilitate the flux of nutrients into the cytoplasm. Transporter proteins that create a channel for substrate transit through the membrane will often have protein regions that extend towards the interior or the exterior of the cell membrane, facilitating nutrient selection and uptake [6–8]. Such protein regions are subject to distinct selective pressures to maximize function given environmental, ecological and physiological constraints. This balance between function, physiology and environment determines marine microbial distribution by restricting growth of populations that cannot compete at low substrate concentrations [4] and

results in genome-wide adaptations to elemental scarcity, particularly nitrogen [9–11]. To meet metabolic demands and remain competitive, microbes that live in low nutrient conditions are predicted to have transporter proteins with optimal affinity for their substrate [12,13], yet there is no clear demonstration of how such ecological circumstances have driven transporter sequence evolution.

At extracellular concentrations of ammonium less than 1 mM, microbes require transport systems such as ammonium transporters (Amts) [14]. Microbial Amts belong to the methylammonia permease (MEP) family of transporter proteins with homologues found in all three domains of life [15]. Crystal structures were first reported for the AmtB protein of *Escherichia coli* [16,17], and the Amt-1 protein of *Archaeoglobus fulgidus* [18]. These proteins consist of 11 membrane-bound α -helices with cytoplasm and periplasm extensions, forming individual channels in a trimer quaternary structure [18–20]. Amts have a history of uncertainty surrounding the mechanism of passive or active transport, as well as the specificity for ammonia (NH_3) and/or ammonium (NH_4^+) [17,21–25]. Recent experiments describe Amt as a NH_4^+/H^+ symporter, actively transporting primarily NH_4^+ with some transport of methylammonium and limited NH_3 passage [26–28]. The preference of NH_4^+ is predicted from models due to the net negative charge of the periplasm extensions of the transporter protein, with NH_3 passing through the transporter channel via deprotonation at a periplasm-facing active site and reprotonation/release at a cytoplasm-facing site [16,26,29,30]. The Amt active site at which NH_4^+ binds in the periplasm has been defined by a highly conserved ‘phenylalanine-gate’ motif, along with tryptophan and serine residues in AmtB [16,17,24]. During the transport of NH_4^+ , the deprotonation-mediated proton concentration increase (and pH decrease) in the periplasm may further an acid-trap mechanism that accumulates NH_4^+ in the periplasm [31], demonstrating the importance of electrochemical properties to the function of these proteins.

Amt homologues can be classified by the presence or absence of a cleavable N-terminal signal peptide [32], which we indicate here with ‘+’ and ‘–’ symbols. ‘Amt+’ possess a cleavable N-terminal signal peptide for translocation into the cytoplasm membrane via the general secretory (Sec) pathway [19]. ‘Amt–’ do not possess the cleavable N-terminal signal peptide and have been suggested to translocate into the cytoplasm membrane via a non-classical secretion pathway [32]. Prokaryotes often encode and express multiple Amt paralogues, indicating subfunctionalization related to optimal function in different substrate concentrations and/or environmental pH [18,27,32–34]. Results from these previous experiments suggest that Amt– has a lower affinity and is used by microbes in higher $[\text{NH}_4^+]$ environments. For both sets of Amt homologues, amino acid distribution is such that cytoplasm extensions have a higher net positive charge (e.g. rich in arginine, histidine and lysine amino acids) compared to periplasm extensions (rich in aspartic acid and glutamic acid), following a ‘positive-inside’ rule of transmembrane proteins [25,26,29,35]. This arrangement creates a dipole moment over the length of the protein. The oppositely charged transporter ends generate an electric field that, when interacting with a positively charged ion, exerts a force that loops externally around the protein (figure 1) and facilitates transport (approx. 2000 Debye for *E. coli* AmtB trimer [29]).

Microbial nutrient uptake alters concentrations of free substrates, making the process an important nutrient sink

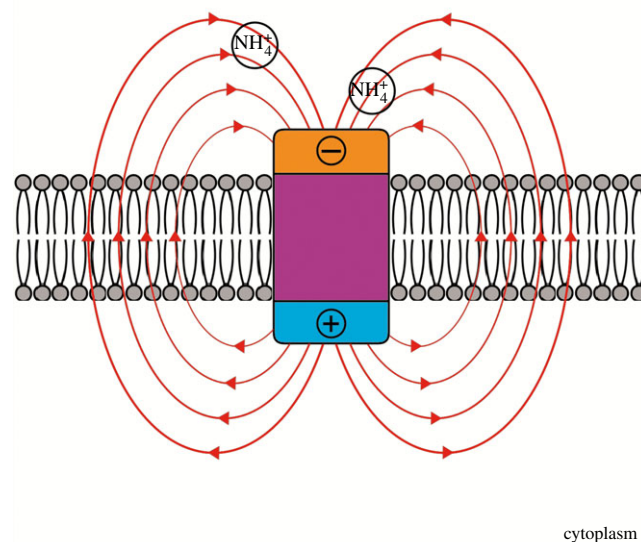


Figure 1. The electric field around Amt facilitates NH_4^+ uptake. The direction of the electric field flows outward from the positively charged end in the cytoplasm, loops around and exits the cell through the surrounding membrane space, then loops back inward towards the negatively charged end in the periplasm. Importantly, this force passes through the periplasm fluid and is thought to both recruit a higher proportion of cations to the periplasm vestibule while inhibiting anion binding, as well as help guide and orient NH_4^+ towards the binding pocket [16,25,29,36]. The hydrophobic properties of the transmembrane channel which requires deprotonation of NH_4^+ and subsequent conductance of NH_3 , selects against the passage of cations that would require replacement for their hydration shell, such as K^+ [16].

in biogeochemical cycles [37]. NH_4^+ is a key component of the nitrogen cycle and a prime example of a nutrient highly influenced by microbes who use it both as an anabolic N source and as an energy source (i.e. ammonia-oxidizing microorganisms). NH_4^+ exists in equilibrium with NH_3 ($\text{H}_2\text{O} + \text{NH}_3 \leftrightarrow \text{OH}^- + \text{NH}_4^+$). At surface ocean pH, temperature, and salinity, approximately 80% of their combined total exists as NH_4^+ and increases as these parameters change with depth [38]. NH_4^+ concentrations in the open ocean peak at the base of the sunlit euphotic zone (>150 nM) then rapidly decrease to vanishingly low concentrations with depth (<5 nM), eventually reaching the limits of direct measurement [39–42]. Low NH_4^+ concentrations have previously been interpreted to indicate diminished relative importance as a nutrient and energy source in the deep ocean [43]. Instead, low concentrations reflect the balance between uptake and supply, with high-affinity NH_4^+ uptake balancing supply. Properties of Amt transporters that impart a competitive advantage at lower concentration environments may help explain the fate of NH_4^+ in the deep ocean.

Here, we use a global marine metagenomic dataset (Tara Oceans [44]) combined with a time-series dataset (Hawai'i Ocean Time-series at Station 'A Long-term Oligotrophic Habitat Assessment' (HOT/ALOHA) [10]) to compare the distribution of Amt sequence types across ocean depths, working under the assumption that deeper depths represent more NH_4^+ limited environments. We focus on three microbial taxa—Marine Group I (MGI) Archaea (formerly Thaumarchaeota and currently proposed as Class Nitrososphaeria within

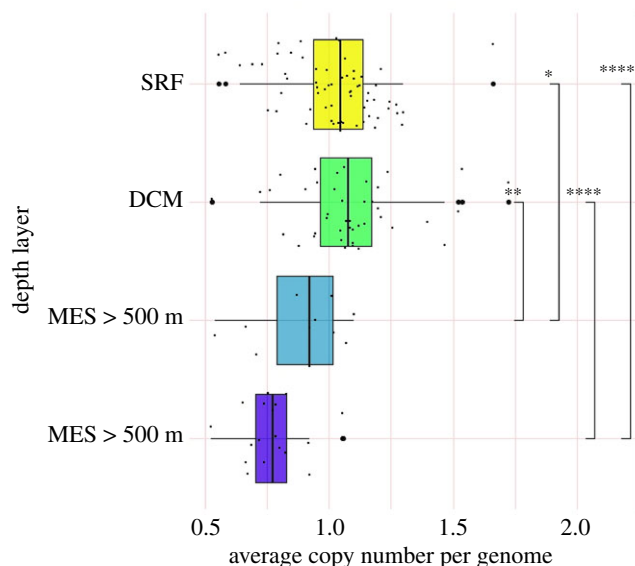


Figure 2. Average microbial *amt* gene copy number per genome decreases with depth in the ocean. Tara samples are separated into four separate depth layers: SRF (Tara SRF and MIX; yellow), DCM (Tara DCM; green), MES < 500 m (Tara MES samples from less than 500 m; blue) and MES > 500 m (Tara MES samples from greater than 500 m; purple). Individual Tara samples are plotted as black points surrounding their corresponding depth layer box plot. To aid in visualization of individual samples, points are offset from their gridlines and outlier samples are marked with a larger bold point on the gridline at their *x*-axis position. Wilcoxon–Mann–Whitney test comparisons and their *p*-values are displayed as brackets with corresponding significance ranges (* ≤ 0.05 , ** ≤ 0.01 , *** ≤ 0.001 , **** ≤ 0.0001).

the Thermoproteota [45]), the gammaproteobacteria SAR86 (clades A, B and E), and the alphaproteobacteria SAR11—that are abundantly represented in both shallow and mesopelagic layers of the water column, as well as globally dispersed [44,46,47]. Little is known of the NH_4^+ affinity of these taxa, owing to the challenge of cultivating relevant representatives from the ocean and the difficulty with determining transport affinities at low substrate concentrations. Insight into their Amt protein sequence properties that conveys relative NH_4^+ affinity could reveal different competition strategies in different ocean layers.

2. Results

Restricting Amt sequence comparisons to within each taxon and Amt type (Amt+ or Amt–) reduced the diversity of amino acid multiple alignment positional homology and facilitated direct comparison between ‘shallow’ (Tara samples labelled surface, deep chlorophyll maximum and mixed; HOT/ALOHA ≤ 175 m) and ‘deep’ (mesopelagic; HOT/ALOHA greater than 175 m) sampled sequences. Our depth boundary of 175 m in HOT/ALOHA samples separates the euphotic zone (shallow) from the non-euphotic zone (deep) [48]. The average copy number of Tara Oceans *amt* sequences relative to prokaryotic single-copy genes decreases with depth in our dataset, with medians ranging from 1.04 copies per genome in surface waters to 0.92 copies per genome below 175 m and decreasing further to 0.77 in samples from below 500 m (figure 2). However, these calculations assume that the diversity of microorganisms and their genomes were sampled to the same extent in all of the

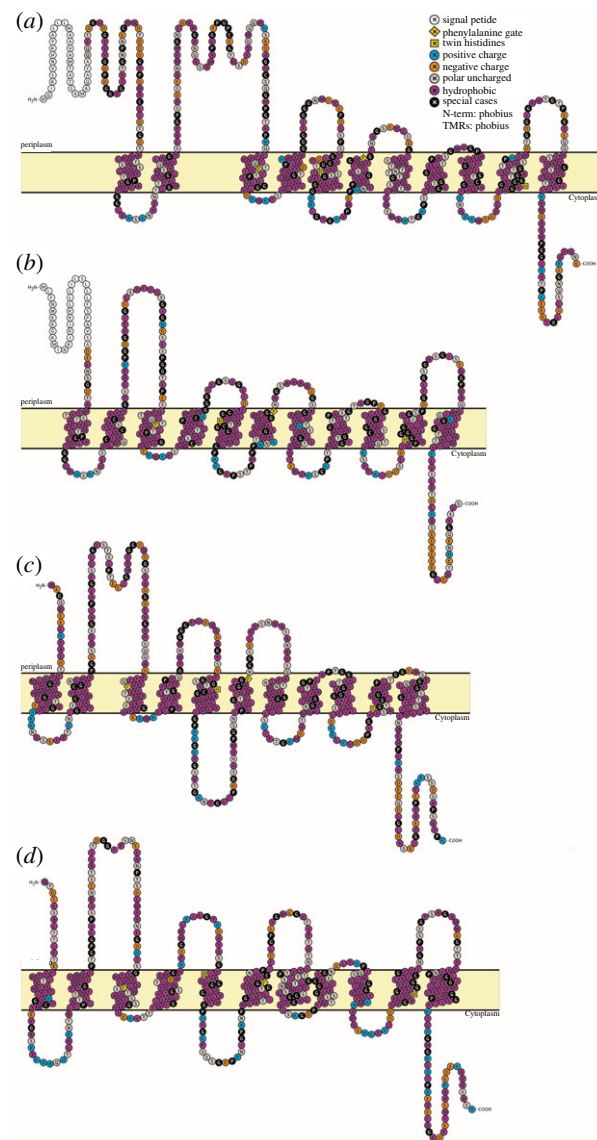


Figure 3. Transmembrane topologies of Amt from the three taxa examined in this study. (a) MGI Amt+ consensus sequence, (b) SAR86 Amt+ consensus sequence, (c) SAR86 Amt– consensus sequence and (d) SAR11 Amt– consensus sequence. Individual amino acids are labelled with their single letter code and colour coded based on side chain properties or their presence in well-characterized sequence motifs (Amt+ signal peptide, white; phenylalanine gate conserved motif, yellow diamond; twin histidine conserved motif, yellow square; positively charged, blue; negatively charged, orange; polar uncharged, grey; hydrophobic, purple; special cases, black). The cytoplasmic membrane is represented as a yellow band that separates the periplasm (top) and cytoplasm (bottom), with periplasm extensions, cytoplasm extensions and transmembrane regions mapped in their respective regions.

collected metagenomes, and therefore our copy number results warrant further validation.

We compared four distinct Amt variants from shallow and deep ocean sample metagenomes: a thaumarchaeal Amt+, both an Amt+ and Amt– from SAR86, and Amt– from SAR11. MGI Amt– and SAR11 Amt+ clades were not abundant enough in both sample depth layers to include for analysis. For each of the Amt comparisons, we created multiple sequence alignments of Amt and used the resulting consensus sequences to create secondary structure topology maps (figure 3a–d), which defined Amt sequence localizations and allowed us to perform Chi-square analysis on

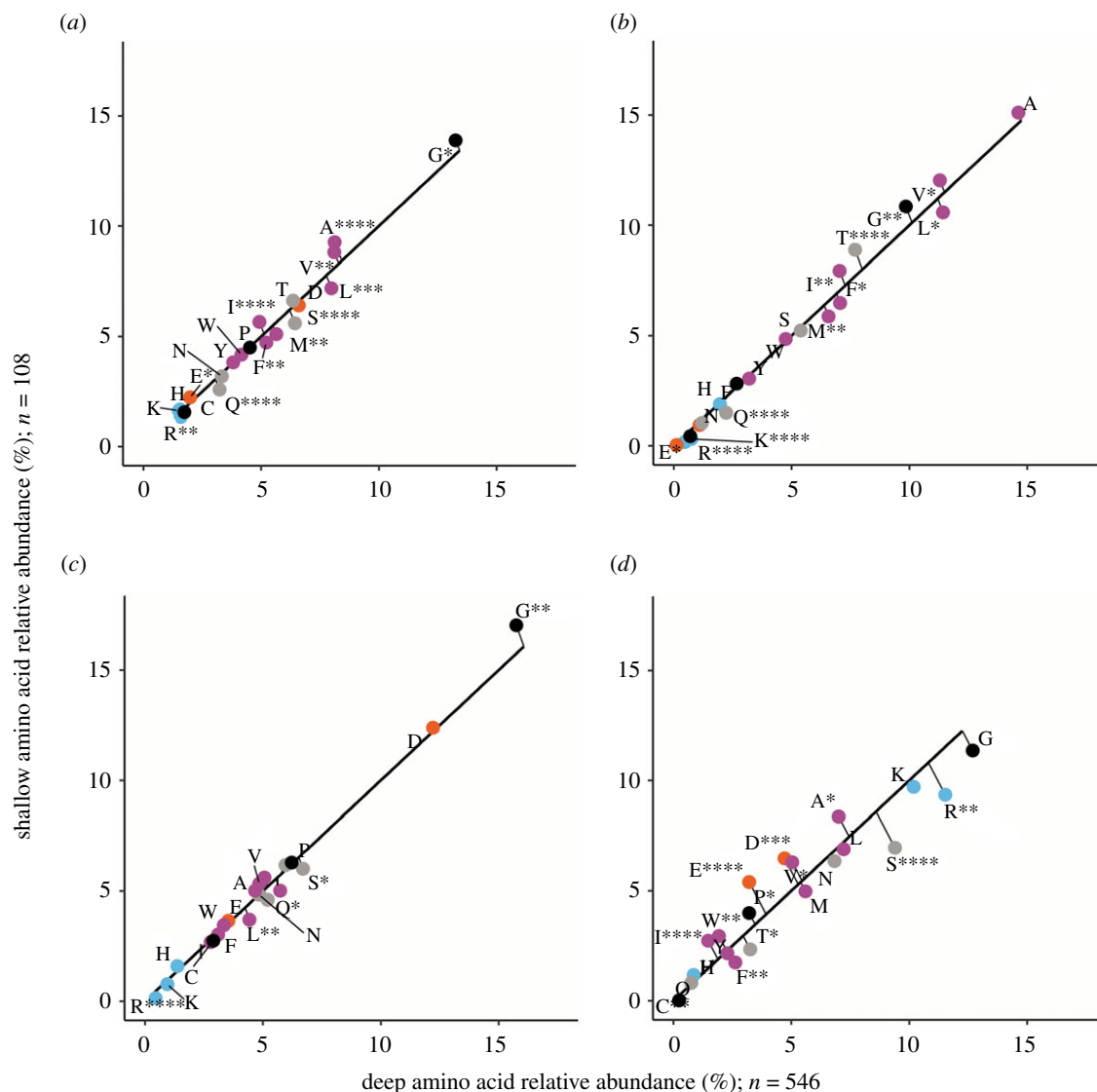


Figure 4. Amino acid usage for different regions of MGI Amt+ sequences: (a) overall protein, (b) the membrane region, (c) the periplasm region and (d) the cytoplasm region. Each graph shares the same axes of amino acid relative abundance, with deep sequences on the x-axis and shallow sequences on the y-axis. The black line represents the expected amino acid abundances if there were no difference in usage between shallow and deep sequences. The points are actual amino acid usage labelled with conventional amino acid single letter codes and coloured by side chain properties, positive (blue), negative (orange), uncharged (grey), hydrophobic (purple) and black (special cases). Points that fall below the expected line are more abundant in deep sequences than in shallow sequences. Plotted points that fall above the expected line are more abundant in shallow sequences than in deep sequences. Significance in the deviation from the expected line was calculated with chi-square analysis, $*\leq 0.05$, $**\leq 0.01$, $***\leq 0.001$, $****\leq 0.0001$.

amino acid compositions (figures 4–7). For the overall Amt alignments, the relative abundances of charged amino acids were low when compared to polar uncharged and hydrophobic amino acids (figures 4a, 5a, 6a and 7a). Overall Amt amino acid usages were greatly influenced by the membrane-bound regions, which are composed mostly of polar uncharged and hydrophobic amino acids (figures 4b, 5b, 6b and 7b). In all of our Amt comparisons, the relative abundances of charged amino acids in the periplasm and cytoplasm extensions exhibit the ‘positive-inside’ rule discussed above, where the net charge of cytoplasm extensions is more positive than the net charge of periplasm extensions. However, for each of our comparisons, the degree to which the rule is followed differs between shallow and deep samples.

The charged amino acid composition of periplasm extensions for both of our Amt+ alignments are similar between shallow and deep samples (table 1; figures 4c and 5c), but cytoplasm extensions from deep samples have an increased positive charge relative to shallow samples (table 1;

figures 4d and 5d). When calculating normalized net charges for cytoplasm extensions at pH 7, a value generally relevant to microbial cytoplasm, MGI Amt+ sequences from deep samples have a charge that is approximately 6.6 charge units more positive than in shallow samples (table 1; calculation described in Methods). In SAR86 Amt+ sequences, cytoplasm extensions have a charge that is approximately 1.2 charge units more positive in deep samples than in shallow samples (table 1). If we then subtract periplasm net charges from cytoplasm net charges to calculate a dipole charge difference, MGI Amt+ sequences from deep samples have a dipole charge difference that is approximately 5.8 charge units greater than in shallow sample sequences (table 1). SAR86 deep sample Amt+ sequences have a similar but less pronounced charge difference that is approximately 1.0 charge units greater than in shallow samples (table 1).

In comparison to the Amt+ type, patterns of charged amino acid variation with depth were different for the Amt– we examined (table 1; figures 6 and 7). In SAR86 Amt– sequences

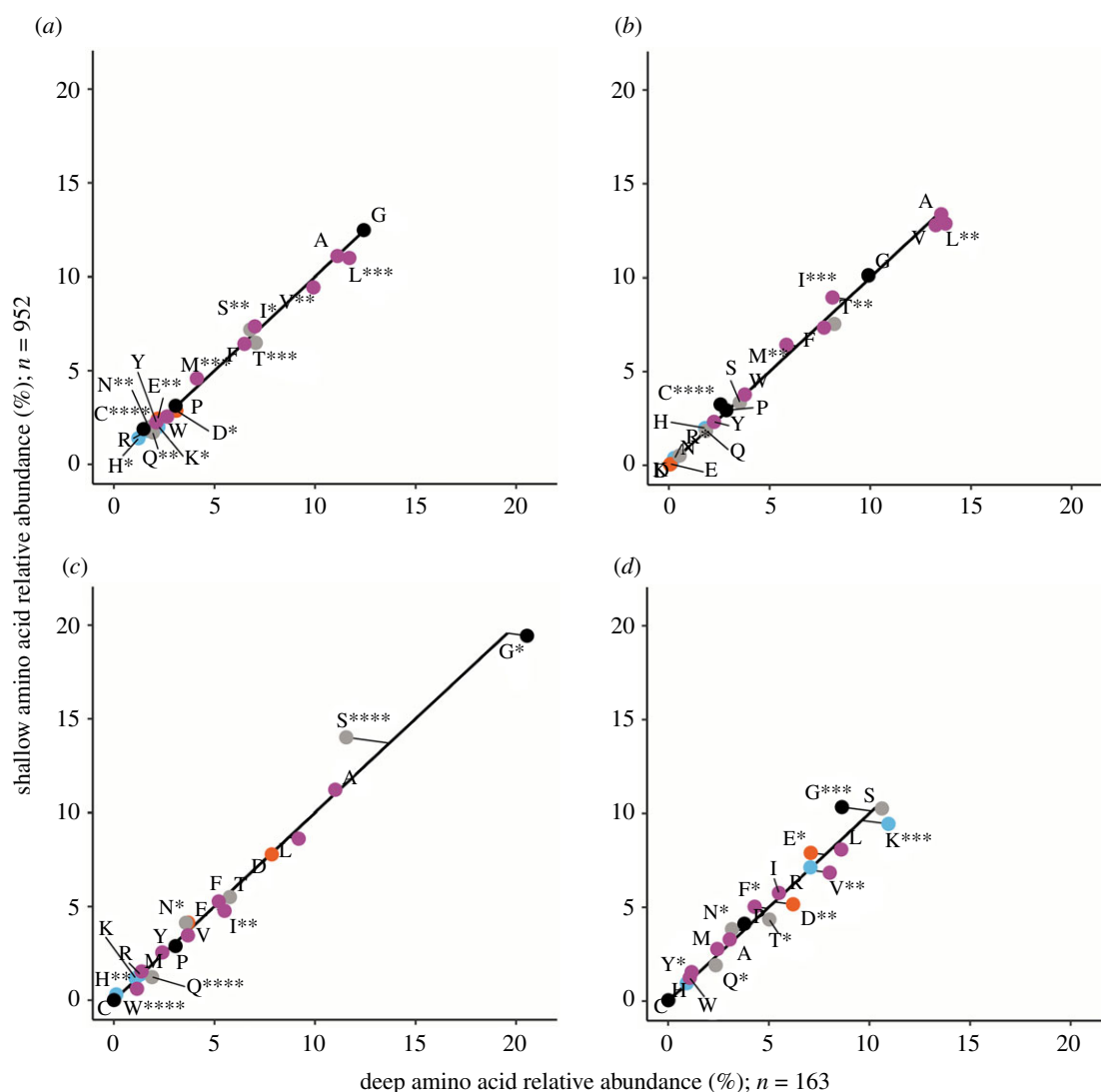


Figure 5. Amino acid usage for different regions of SAR86 Amt⁺ sequences. Panels, axes and points are as in figure 4.

(figure 6), most of the net charge variation again occurs in cytoplasm extensions but also with some difference in periplasm extensions. Cytoplasm extensions in SAR86 Amt[−] from deep samples are approximately 4.8 charge units less positive than shallow samples, and periplasm extensions are approximately 1.8 charge units more positive in deep samples (table 1). If we subtract periplasm net charges from cytoplasm net charges, SAR86 Amt[−] sequences from deep samples have a dipole charge difference that is approximately 6.6 charge units less than shallow sample sequences (table 1). In SAR11 Amt[−] sequences, most of the net charge difference between shallow and deep samples occurs in periplasm extensions, which are approximately 0.8 charge units more positive in deep samples than in shallow samples (table 1). SAR11 Amt[−] sequences have a similar but less pronounced dipole charge difference between oppositely facing extensions to that of SAR86 Amt[−], with a value that is approximately 0.8 charge units greater in shallow samples than in deep samples due to minimal cytoplasm extension differences (table 1).

In addition to the charge differences described above, each Amt comparison differs in the counts of sequences from shallow or deep samples (figures 4–7), the magnitude of the dipole charge difference between shallow and deep samples (e.g. 22.27 and 28.1 charge units for MGI Amt⁺, respectively; table 1), and the utilization of amino acids that

amount to net charge differences (figures 4–7). Each Amt in our comparisons utilizes a different distribution of charged amino acids while maintaining cytoplasm extensions that are more positive than periplasm extensions. Chi-square tests of homogeneity on the periplasm and cytoplasm charged amino acid distributions in all four deep and shallow sample comparisons have p -values < 0.001 , indicating amino acid abundances of deep and shallow Amt sequences are composed of different amino acid profiles.

3. Discussion

Our study aimed to determine whether or not functional adaptations to low NH_4^+ concentrations could be discerned from sequence data, using the Amt transporter as a test case. We did not identify any Amt amino acid sequence regions that are specific to shallow or deep samples in any of the lineages within our focus. However, we did observe differences in the Amt amino acid usage between sequences from shallow and deep samples. By increasing the proportion of negatively charged amino acids in the periplasm, organisms could theoretically increase the Debye strength of the electric field surrounding Amt, increasing the effective range of their attractive force and thereby their substrate



It may seem counterintuitive for a transmembrane transporter protein to have higher substrate affinity by adaptation of regions facing away from substrate but it is an elegant solution to increasing NH_4^+ recruitment without altering substrate binding and deprotonation environments. Like many proteins, the binding pocket size, shape and charge of Amt_s at the periplasm mouth of the transmembrane region is a critical component of NH_4^+ recruitment and specificity [8,36]. Maintaining the amino acid tertiary structure of the Amt binding site may be an evolutionary barrier that impedes large changes in periplasm extension amino acid usage.

disparity from shallow to deep ocean samples and the difference in SAR86 Amt+ was significant but relatively minimal (table 1). This could be due to greater selective pressure for attracting NH_4^+ for catabolic demands compared with solely biosynthetic needs. Higher affinity AmtS would also help marine microbes, especially MGI, meet NH_4^+ influx demands to offset the loss of NH_3 due to high membrane permeability and a concentration gradient that favours diffusion out of the cell [14]. If permeation of NH_3 is great enough in MGI, it may create localized NH_3 concentrations for oxidation by membrane-bound ammonium monooxygenase [50]. If Amt+ sequences in the deep ocean are exhibiting our observed exaggerations of dipole charge in response to competitive evolutionary forces, then that would indicate NH_4^+ in the deep ocean is in high demand and its scarcity is due to efficient uptake by microbes expressing such AmtS. Similarly, if a large Amt dipole charge exaggeration is the result of competition for a limited amount of NH_4^+ , then a small dipole charge exaggeration (as seen in SAR86 Amt+) could mean that environmental NH_4^+ concentration is not a strong selection factor for growth or that these organisms rely on the transport of other anabolic sources, such as dissolved organic matter [51,52]. A stronger electric field may even become inhibitory if it over-attracts substrate (toxicity and decreased flux [13,53]) and non-substrate

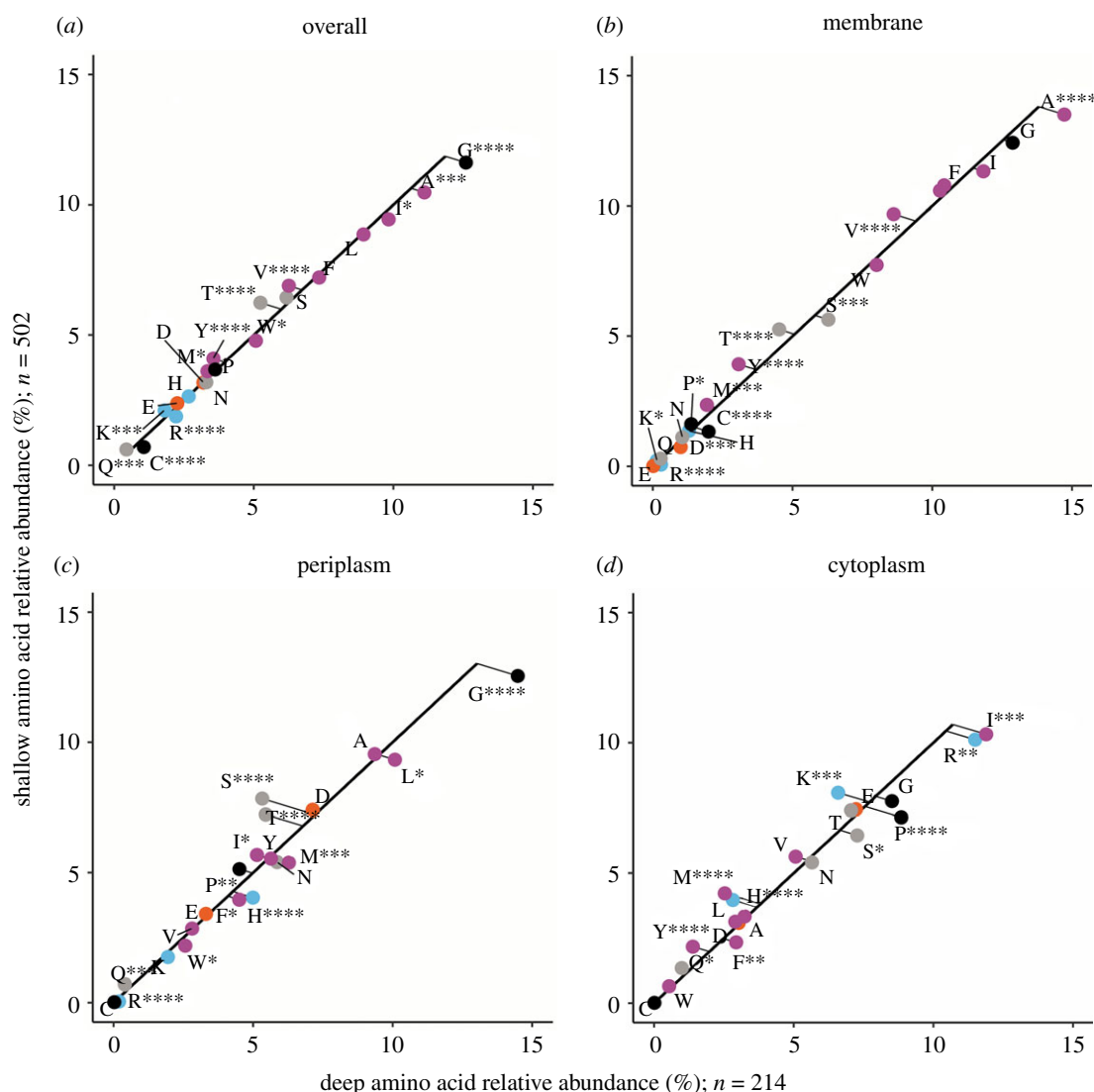


Figure 7. Amino acid usage for different regions of SAR11 Amt[−] sequences. Panels, axes and points are as in figure 4.

(competitive inhibition [27]). Alternatively, a large dipole charge exaggeration may allow MGI to compensate for the scarcity of energy in the deep ocean, which limits the amount of Amt[−] (and total proteins) that can be produced by MGI cells to increase NH_4^+ uptake [54].

In culture, *Nitrosopumilus maritimus* SCM1 (MGI) Amt[−] transcripts were reduced during NH_4^+ starvation (nM concentration), while Amt⁺ transcripts were unchanged [34]. *N. maritimus* SCM1 are known to be well-adapted to acquiring NH_4^+ in low substrate environments, having a high affinity with a Michaelis constant (K_m) of 132 nM total NH_4^+ [33]. Our low counts of MGI Amt[−] sequences (too low for Chi-square analysis) from deep samples are consistent with findings that Amt[−] may not be present at all in deep ocean MGI [55], despite being present in genomes from cultured MGI [56,57].

The charge distributions that we observe for the two Amt[−] containing taxa have an opposite direction of exaggeration than the Amt⁺ containing taxa. That is, they both have an increased dipole charge distribution in shallow sample sequences relative to deep samples. A low affinity transporter (Amt[−]) might not be expected to evolve higher affinity variants in low substrate conditions, such as the deep ocean if a high-affinity transporter (Amt⁺) is already encoded within the genome. The Amt[−] dipole charge difference that we observed is most prominent in SAR86, with members of

the SAR11 clade having the smallest difference between deep and shallow samples (minimal difference but significant; table 1). Under our competition premise, an increased dipole charge distribution in shallow sample sequences relative to deep would mean that NH_4^+ acquisition is more of a limiting factor for growth in the shallow ocean for these taxa than in the deep. Since NH_4^+ concentration decreases with depth, this suggests that SAR11 and SAR86 in the deep ocean are limited by some factor other than NH_4^+ . At least some clades of SAR11 and SAR86 are capable of proteorhodopsin-conferred photo-heterotrophy, using light to generate ATP and enhance nutrient uptake for growth [51,58–61]. Without this energy-harvesting process available in the deep ocean, the chemoheterotrophic SAR11 and SAR86 could be limited by organic carbon availability, not nitrogen. It may even be disadvantageous to have higher affinity Amt[−] (both Amt[−] and Amt⁺) that spend limited energy bringing in excess NH_4^+ that cannot be used for growth. Moreover, increased affinity does not necessarily equate to increased NH_4^+ uptake rate. Optimal uptake kinetics models imply a trade-off between increased affinity and maximum uptake velocity for whole cells, which may mean that these organisms increase membrane transporter density or deplete intracellular NH_4^+ to free enzyme active sites as means for increased uptake [62].

Table 1. Normalized net amino acid charge distributions across periplasm and cytoplasm consensus sequence regions of MGI Amt+, SAR86 Amt+, SAR86 Amt– and SAR11 Amt– from deep and shallow samples. Net charges are calculated from charged amino acid relative abundances as described in the methods and dipole charge difference is defined as: cytoplasm net charge – periplasm net charge. Chi-square tests of homogeneity on the periplasm and cytoplasm charged amino acid distributions in all four deep and shallow sample comparisons have *p*-values < 0.001.

	periplasm net charge	cytoplasm net charge	dipole charge difference
MGI Amt+			
deep	–14.22	13.88	28.1
shallow	–14.96	7.31	22.27
difference	0.74	6.57	5.83
SAR86 Amt+			
deep	–9.16	4.81	13.97
shallow	–9.36	3.6	12.96
difference	0.2	1.21	1.01
SAR86 Amt–			
deep	–9.65	–1.03	8.62
shallow	–11.4	3.81	15.21
difference	1.75	–4.84	–6.59
SAR11 Amt–			
deep	–7.8	8.11	15.91
shallow	–8.61	8.06	16.67
difference	0.81	0.05	–0.76

SAR86 also appears to be more dependent on NH_4^+ acquisition than SAR11. So far, no urease genes have been found in SAR86 genomes [63], but have been found in SAR11 [64]. SAR86 genomes also have low counts of ABC-type transporter genes that could be utilized for amino acid uptake [51], uptake that was indeed measured to be low in ocean waters [65]. By contrast, SAR11 genomes contain many amino acid transporter genes that have high affinity and are multifunctional [66,67], and SAR11 are responsible for up to 50% of amino acid assimilation in ocean surface waters [68]. SAR11's ability to efficiently scavenge N from multiple sources could be why there is little difference between shallow and deep sample sequences. For SAR86, the combination of a high-affinity Amt+ and a low-affinity Amt– with an exaggerated dipole in shallow samples could both be needed to meet N requirements.

The high abundance of lysine and aspartic acid that we see in SAR86 Amts (figures 5 and 6) could be a result of necessity, since SAR86A may be deficient in arginine and histidine with an excess of aspartic acid. SAR86A, a clade of SAR86, lack proteins required for histidine and arginine synthesis pathways which utilizes aspartic acid as a precursor [51]. In marine microorganisms with streamlined genomes, there is a trend of increased compositional bias for nucleotide and amino acids of lower N content, such as the substitution of lysine for arginine [9,69]. Lower N content compositional bias is thought to reduce the amount of N needed for cell

growth and replication [70], but further study is needed to show the extent of this trend specifically in SAR86 clades. In our study, SAR86A represented approximately 8% of SAR86 Amt– shallow sequences, approximately 4% of SAR86 Amt– deep sequences, approximately 10% of Amt+ shallow sequences, and 0% of Amt+ deep sequences. These percentages are not definite, since approximately 73% of Amt+ and approximately 91% of Amt– SAR86 annotations were not clade specific. However, it is interesting that Amts in SAR86A maintain the 'positive-inside' rule and appear to evolve a charge exaggeration even while auxotrophic for some charged amino acids, implying that charge properties of Amt must be crucial for function.

While we are unable to quantify actual changes in the dipole moment strength among Amt variants, which would require crystal structure tertiary coordinates of charged amino acids in order to be calculated [49], we are able to make qualitative comparisons of dipole distribution differences between taxa, ocean layers and Amt types. In all clades, the major differences in amino acid distribution occur in the cytoplasm extensions, which are collectively more positively charged than their periplasm extensions. An interesting exception is the cytoplasm-facing C-terminus tail, which has a net negative charge [19]. This negatively charged tail is modelled to interact with positively charged cytoplasm extensions of neighbouring Amt monomers, linking them into their trimer quaternary structure as well as facilitating the binding of regulatory GlnK or GlnK-like proteins [18,19,71,72]. When C-terminal tails are omitted from our analysis to confirm that their absence in partial sequences are not the sole cause of our observations, the observed disparity between deep and shallow net charges are altered but not negated. Intriguingly, only Amt– have an extended C-terminal tail and an adjacent *glnK* gene in the genomes of ammonia-oxidizing archaea [32]. If similar features hold true for Amt– of other taxa, it could mean that Amt– are more likely to have a lesser dipole disparity than Amt+ due to the negative charge of extended C-terminal tails.

To speculate, over evolutionary time, Amt electric fields could be tunable to specific NH_4^+ concentrations and/or ecological conditions; possessing a transporter that is properly tuned to environmental conditions offers a competitive advantage. Possessing multiple variants of Amt in a genome may be advantageous for populations that need to regulate NH_4^+ transport in fluctuating conditions [32]. Our results suggest a stronger Amt electric field helps competing populations only if NH_4^+ acquisition is limiting growth. Other membrane transporter proteins could utilize similar electric field strategies to compete for growth-limiting ion substrates. Our work will inform future examination of dipole charge distribution with electric field strength and substrate affinity measurements, testing the expectations of exaggerated dipole charge distribution leading to increased NH_4^+ recruitment.

4. Methods

We used data from 243 Tara Oceans [44] and 165 HOT/ALOHA metagenome samples [10]. We found 32 566 partial and complete predicted protein-coding *amt* sequences from pre-existing metagenome unbinned contig assemblies (electronic supplementary material, file S1) with a DIAMOND (v. 0.9.24.125) [73] blastx search against a curated set of 52 bacterial and

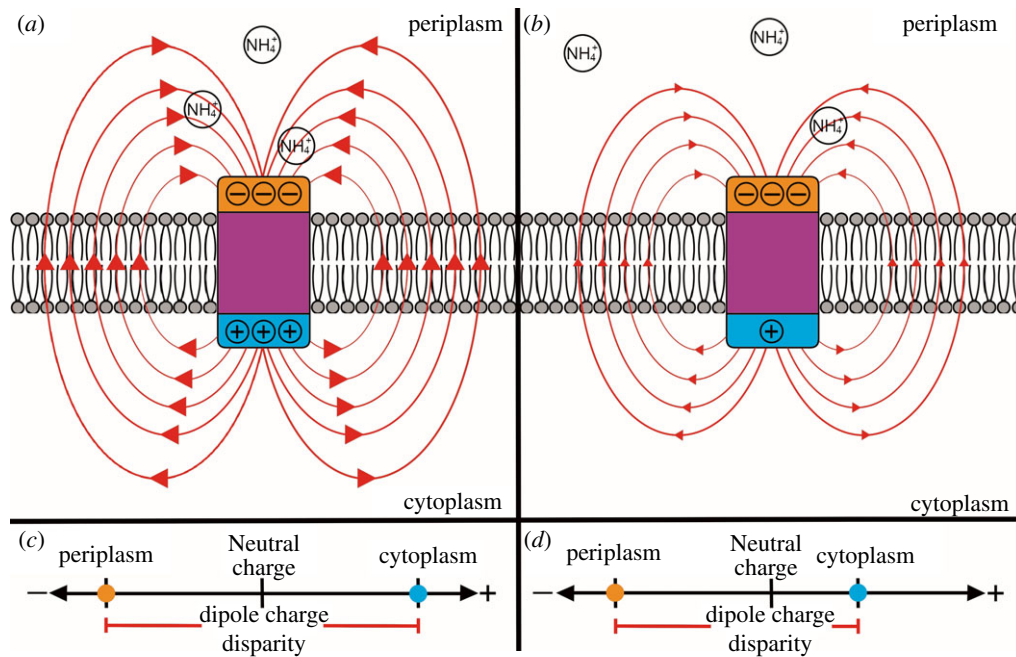


Figure 8. Schematic of Amt electric fields created by dipole amino acid charge distributions. The charge disparity of Amt is shown between the positively charged cytoplasm (blue) and negatively charged periplasm (orange) regions, separated by the hydrophobic membrane (purple) region and lipid bilayer. With equal periplasm charges, a large dipole charge disparity created by a strongly positive cytoplasm charge (a) and small dipole charge disparity created by a less positive cytoplasm charge (b) are compared to visualize the effects on the electric field. Representations of large and small charge disparities between periplasm and cytoplasm regions are plotted along an axis in (c) and (d), respectively, with the membrane region not plotted. Red arrow lines show the direction and approximate paths of the electric field as they would act on positively charged ions. Positively charged ammonium ions in the periplasm are depicted to be attracted towards the Amt periplasm region by the electric field. For simplicity, any electric field paths that flow through the Amt membrane region are not depicted, since the strongly hydrophobic properties of the membrane region would inhibit the travel of charged ions, and thus the influence of the field.

archaeal UniProt [74] Amt sequences, with an E-value cutoff of 0.001. Taxonomy classifications of the *amt* sequences were assigned with a DIAMOND blastx search, E-value cutoff of 1×10^{-20} , against the NCBI non-redundant protein database. The annotated predicted protein-coding *amt* sequences were translated to Amt amino acid sequences with TranslatorX [75]. The Amt sequences were then clustered with CD-HIT (v. 4.8.1) [76] iteratively for clustering cutoffs of 0.5 to 1.0 to confirm sequence grouping by taxonomy annotation, which can have varying levels of conservation between taxa. Within our whole Amt dataset, approximately 75% of Amt sequences are from Tara samples. Within the three taxa of our focus, approximately 80% of Amt sequences are from Tara samples.

amt average copy numbers per genome in the water column were estimated by comparing *amt* abundances in our Tara Oceans metagenome search data relative to 10 prokaryotic single-copy genes suited for metagenomic applications (COG0012, COG0016, COG0018, COG0172, COG0215, COG0495, COG0525, COG0533, COG0541, COG0552) [77], using a DIAMOND E-value of 1×10^{-20} and UniProt single-copy gene sequences. The number of genomes in each metagenome was estimated by calculating the average number of protein sequences assigned to the 10 prokaryotic single-copy COGs. The average number of *amt* sequences per genome was calculated by dividing the number of collected *amt* sequences by the estimated number of genomes. *amt* average copy numbers per genome were plotted in R (ggplot2) [78]. For these calculations, water column samples were separated into four depth layers, surface and mixed layer samples (Tara SRF and MIX), deep chlorophyll maximum (DCM) samples, mesopelagic (MES) samples < 500 m, and MES greater than 500 m. Wilcoxon–Mann–Whitney tests with post hoc Bonferroni adjustments for multiple comparisons were used to

test *amt* average copy number depth layer comparisons for significance in R [79].

We then investigated Amt sequences separated into ‘shallow’ (Tara SRF, MIX, DCM, and HOT/ALOHA ≤ 175 m) and ‘deep’ (Tara MES and HOT/ALOHA > 175 m) ocean layers looking for conserved amino acid positions or patterns in their sequence alignments (MAFFT v. 7.407) [80] that correspond to sample depth, as well as amino acid composition. Through multiple alignment of MGI, SAR11 and SAR86 variant clades and secondary structure prediction (Protter v. 1.0) [81] of consensus sequences, we isolated our analysis to specific regions of the protein sequences: periplasm-facing extensions (excluding the N-terminal signal peptide region in Amt+), cytoplasm-facing extensions, and membrane-bound regions. Protter secondary structure prediction of consensus sequences utilizes Phobius [82] to predict signal peptides and transmembrane regions. To avoid extending consensus sequences with residues that do not reflect the properties of the whole Amt variant clade, multiple alignment columns were discarded from the consensus sequences if they had low representation, with less than 5% of the aligned sequences containing a residue at the removed column position. Removed columns are marked as ‘NA’ in the ‘Threshold column counts’ tabs of electronic supplementary material, files S2–S5. We then calculated the relative abundance of amino acids per sequence. A chi-square test of homogeneity between shallow and deep sample abundances of amino acids, where the null hypothesis assumes identical distribution, was used to determine if the distributions of cytoplasm- and periplasm-extension charged amino acids (arginine, histidine, lysine, aspartic acid and glutamic acid) differed, confirming two separate groups of sequences with all comparisons indicating a *p*-value < 0.001 (electronic

supplementary material, files S2–S5). Relative abundance of individual amino acids per total amino acids for shallow and deep sequences within each region were compared and plotted in R (ggplot2). Chi-square goodness of fit was used to test the significance of individual amino acid relative abundances per total amino acids, where the null hypothesis assumes no difference in relative abundance between shallow and deep Amt sequences as the expected outcome (electronic supplementary material, files S2–S5).

Net charges were calculated from the percentages of each charged amino acid in cytoplasm and periplasm regions to normalize count information in both shallow and deep samples. At pH 7, arginine, histidine, lysine, aspartic acid and glutamic acid have charges of approximately 1, 0.1, 1, –1 and –1, respectively [83]. These amino acid charges were multiplied by their normalized percentages in periplasm and cytoplasm regions for both shallow and deep samples, yielding normalized net charges and differences that are summarized in table 1.

Data accessibility. All original sequence data are public data and have been previously published elsewhere. Sequences that were used for

this work as a result of alignment searching and all spreadsheets that contain amino acid counts and calculations are available as electronic supplementary material [84].

Authors' contributions. M.K.: data curation, formal analysis, investigation, methodology, project administration, visualization, writing—original draft, writing—review and editing; S.P.: conceptualization, funding acquisition, writing—review and editing; T.A.R.: conceptualization, funding acquisition, writing—review and editing; A.E.S.: conceptualization, funding acquisition, writing—original draft, writing—review and editing.

All authors gave final approval for publication and agreed to be held accountable for the work performed therein.

Conflict of interest declaration. We declare we have no competing interests.

Funding. This work was supported by The Gordon and Betty Moore Foundation Marine Microbiology Initiative (award GBMF5514) to T.A.R., A.E.S. and S.P. Additional support was provided by the United States National Science Foundation (OCE-1924512) to A.E.S. Use was made of computational facilities purchased with funds from the United States National Science Foundation (CNS-1725797) and administered by the Center for Scientific Computing (CSC). The CSC is supported by the California NanoSystems Institute and the Materials Research Science and Engineering Center (MRSEC; NSF DMR-1720256) at University of California, Santa Barbara.

Acknowledgements. We thank Barbara Bayer for feedback on the manuscript.

References

- Brown CJ, Todd KM, Rosenzweig RF. 1998 Multiple duplications of yeast hexose transport genes in response to selection in a glucose-limited environment. *Mol. Biol. Evol.* **15**, 931–942. (doi:10.1093/oxfordjournals.molbev.a026009)
- Milner DS *et al.* 2019 Environment-dependent fitness gains can be driven by horizontal gene transfer of transporter-encoding genes. *Proc. Natl Acad. Sci. USA* **116**, 5613–5622. (doi:10.1073/pnas.1815994116)
- Bernhardt JR, Kratina P, Pereira AL, Tamminen M, Thomas MK, Narwani A. 2020 The evolution of competitive ability for essential resources. *Phil. Trans. R. Soc. B* **375**, 20190247. (doi:10.1098/rstb.2019.0247)
- Moore CM *et al.* 2013 Processes and patterns of oceanic nutrient limitation. *Nat. Geosci.* **6**, 701–710. (doi:10.1038/ngeo1765)
- Song H, Bremer BJ, Hinds EC, Raskutti G, Romero PA. 2021 Inferring protein sequence–function relationships with large-scale positive-unlabeled learning. *Cell Syst.* **12**, 92–101. (doi:10.1016/j.cels.2020.10.007)
- Hilty C, Winterhalter M. 2001 Facilitated substrate transport through membrane proteins. *Phys. Rev. Lett.* **86**, 5624–5627. (doi:10.1103/PhysRevLett.86.5624)
- Mahendran KR *et al.* 2010 Molecular basis of enrofloxacin translocation through OmpF, an outer membrane channel of *Escherichia coli*: when binding does not imply translocation. *J. Phys. Chem. B* **114**, 5170–5179. (doi:10.1021/jp911485k)
- Pagliara S, Dettmer SL, Keyser UF. 2014 Channel-facilitated diffusion boosted by particle binding at the channel entrance. *Phys. Rev. Lett.* **113**, 048102. (doi:10.1103/PhysRevLett.113.048102)
- Giovannoni SJ, Cameron Thrash J, Temperton B. 2014 Implications of streamlining theory for microbial ecology. *ISME J.* **8**, 1553–1565. (doi:10.1038/ismej.2014.60)
- Mende DR, Bryant JA, Aylward FO, Eppley JM, Nielsen T, Karl DM, DeLong EF. 2017 Environmental drivers of a microbial genomic transition zone in the ocean's interior. *Nat. Microbiol.* **2**, 1367–1373. (doi:10.1038/s41564-017-0008-3)
- Shenhav L, Zeevi D. 2020 Resource conservation manifests in the genetic code. *Science* **370**, 683–687. (doi:10.1126/science.aaz9642)
- Button DK. 1991 Biochemical basis for whole-cell uptake kinetics: specific affinity, oligotrophic capacity, and the meaning of the Michaelis constant. *Appl. Environ. Microbiol.* **57**, 2033–2038. (doi:10.1128/aem.57.7.2033-2038.1991)
- Pagliara S, Schwall C, Keyser UF. 2013 Optimizing diffusive transport through a synthetic membrane channel. *Adv. Mat.* **25**, 844–849. (doi:10.1002/adma.201203500)
- Kleiner D. 1985 Bacterial ammonium transport. *FEMS Microbiol. Lett.* **32**, 87–100. (doi:10.1111/j.1574-6968.1985.tb01185.x)
- McDonald TR, Dietrich FS, Lutzoni F. 2011 Multiple horizontal gene transfers of ammonium transporters/ammonia permeases from prokaryotes to eukaryotes: toward a new functional and evolutionary classification. *Mol. Biol. Evol.* **29**, 51–60. (doi:10.1093/molbev/msr123)
- Khademi S, O'Connell J, Remis J, Robles-Colmenares Y, Miercke LJ, Stroud RM. 2004 Mechanism of ammonia transport by Amt/MEP/Rh: structure of AmtB at 1.35 Å. *Science* **305**, 1587–1594. (doi:10.1126/science.1101952)
- Zheng L, Kostrewa D, Bernèche S, Winkler FK, Li X-D. 2004 The mechanism of ammonia transport based on the crystal structure of AmtB of *Escherichia coli*. *Proc. Natl Acad. Sci. USA* **101**, 17 090–17 095. (doi:10.1073/pnas.0406475101)
- Andrade SL, Dickmanns A, Ficner R, Einsle O. 2005 Crystal structure of the archaeal ammonium transporter Amt-1 from *Archaeoglobus fulgidus*. *Proc. Natl Acad. Sci. USA* **102**, 14 994–14 999. (doi:10.1073/pnas.0506254102)
- Thomas GH, Mullins JG, Merrick M. 2000 Membrane topology of the Mep/Amt family of ammonium transporters. *Mol. Microbiol.* **37**, 331–344. (doi:10.1046/j.1365-2958.2000.01994.x)
- Blakey D, Leech A, Thomas GH, Coutts G, Findlay K, Merrick M. 2002 Purification of the *Escherichia coli* ammonium transporter AmtB reveals a trimeric stoichiometry. *Biochem. J.* **364**, 527–535. (doi:10.1042/bj20011761)
- Soupe E, He L, Yan D, Kustu S. 1998 Ammonia acquisition in enteric bacteria: physiological role of the ammonium/methylammonium transport B (AmtB) protein. *Proc. Natl Acad. Sci. USA* **95**, 7030–7034. (doi:10.1073/pnas.95.12.7030)
- Soupe E, Lee H, Kustu S. 2002 Ammonium/methylammonium transport (Amt) proteins facilitate diffusion of NH₃ bidirectionally. *Proc. Natl Acad. Sci. USA* **99**, 3926–3931. (doi:10.1073/pnas.062043799)
- Lupo D, Li X-D, Durand A, Tomizaki T, Cherif-Zahar B, Matassi G, Merrick M, Winkler FK. 2007 The 1.3-Å resolution structure of *Nitrosomonas europaea* Rh50 and mechanistic implications for NH₃ transport by Rhesus family proteins. *Proc. Natl Acad. Sci. USA* **104**, 19 303–19 308. (doi:10.1073/pnas.0706563104)

24. Javelle A, Lupo D, Ripoché P, Fulford T, Merrick M, Winkler FK. 2008 Substrate binding, deprotonation, and selectivity at the periplasmic entrance of the *Escherichia coli* ammonia channel AmtB. *Proc. Natl Acad. Sci. USA* **105**, 5040–5045. (doi:10.1073/pnas.0711742105)
25. Akgun U, Khademi S. 2011 Periplasmic vestibule plays an important role for solute recruitment, selectivity, and gating in the Rh/Amt/MEP superfamily. *Proc. Natl Acad. Sci. USA* **108**, 3970–3975. (doi:10.1073/pnas.1007240108)
26. Ullmann RT, Andrade SL, Ullmann GM. 2012 Thermodynamics of transport through the ammonium transporter Amt—1 investigated with free energy calculations. *J. Phys. Chem. B* **116**, 9690–9703. (doi:10.1021/jp305440f)
27. Wacker T, Garcia-Celma JJ, Lewé P, Andrade SL. 2014 Direct observation of electrogenic NH₄⁺ transport in ammonium transport (Amt) proteins. *Proc. Natl Acad. Sci. USA* **111**, 9995–10000. (doi:10.1073/pnas.1406409111)
28. Monier A *et al.* 2017 Host-derived viral transporter protein for nitrogen uptake in infected marine phytoplankton. *PNAS* **114**, E7489–E7498. (doi:10.1073/pnas.1708097114)
29. Bostick DL, Brooks III CL. 2007 Deprotonation by dehydration: the origin of ammonium sensing in the AmtB channel. *PLoS Comput. Biol.* **3**, 0231–0246. (doi:10.1371/journal.pcbi.0030022)
30. Ariz I *et al.* 2018 Nitrogen isotope signature evidences ammonium deprotonation as a common transport mechanism for the AMT-Mep-Rh protein superfamily. *Sci. Adv.* **4**, eaar3599. (doi:10.1126/sciadv.aar3599)
31. Weidinger K, Neuhaus B, Gilch S, Ludewig U, Meyer O, Schmidt I. 2007 Functional and physiological evidence for a Rhesus-type ammonia transporter in *Nitrosomonas europaea*. *FEMS Microbiol. Lett.* **273**, 260–267. (doi:10.1111/j.1574-6968.2007.00805.x)
32. Offre P, Kerou M, Spang A, Schleper C. 2014 Variability of the transporter gene complement in ammonia-oxidizing archaea. *Trends Microbiol.* **22**, 665–675. (doi:10.1016/j.tim.2014.07.007)
33. Martens-Habbena W, Berube PM, Urakawa H, de la Torre JR, Stahl DA. 2009 Ammonia oxidation kinetics determine niche separation of nitrifying Archaea and Bacteria. *Nature* **461**, 976–979. (doi:10.1038/nature08465)
34. Nakagawa T, Stahl DA. 2013 Transcriptional response of the archaeal ammonia oxidizer *Nitrosopumilus maritimus* to low and environmentally relevant ammonia concentrations. *Appl. Environ. Microbiol.* **79**, 6911–6916. (doi:10.1128/AEM.02028-13)
35. von Heijne G. 1986 The distribution of positively charged residues in bacterial inner membrane proteins correlates with the trans-membrane topology. *EMBO J.* **5**, 3021–3027. (doi:10.1002/j.1460-2075.1986.tb04601.x)
36. Nygaard TP, Rovira C, Peters GH, Jensen MØ. 2006 Ammonium recruitment and ammonia transport by *E. coli* ammonia channel AmtB. *Biophys. J.* **91**, 4401–4412. (doi:10.1529/biophysj.106.089714)
37. Kuypers MMM, Marchant HK, Kartal B. 2018 The microbial nitrogen-cycling network. *Nat. Rev. Microbiol.* **16**, 263–276. (doi:10.1038/nrmicro.2018.9)
38. Bell TG, Johnson MT, Jickells TD, Liss PS. 2007 Ammonia/ammonium dissociation coefficient in seawater: a significant numerical correction. *Environ. Chem.* **4**, 183–186. (doi:10.1071/EN07032)
39. Brzezinski MA. 1988 Vertical distribution of ammonium in stratified oligotrophic waters. *Limnol. Oceanogr.* **33**, 1176–1182. (doi:10.4319/lo.1988.33.5.1176)
40. Karl DM, Bidigare RR, Church MJ, Dore JE, Letelier RM, Mahaffey C, Zehr JP. 2008 The nitrogen cycle in the North Pacific trades biome: an evolving paradigm. In *Nitrogen in the Marine Environment*, 2nd edition (ed. DG Capone), pp. 705–769. Amsterdam, The Netherlands: Elsevier.
41. Raimbault P, Garcia N. 2008 Evidence for efficient regenerated production and dinitrogen fixation in nitrogen-deficient waters of the South Pacific Ocean: impact on new and export production estimates. *Biogeosciences* **5**, 323–338. (doi:10.5194/bg-5-323-2008)
42. Santoro AE, Sakamoto CM, Smith JM, Plant JN, Gehman AL, Worden AZ, Johnson KS, Francis CA, Casciotti KL. 2013 Measurements of nitrite production in and around the primary nitrite maximum in the central California Current. *Biogeosciences* **10**, 7395–7410. (doi:10.5194/bg-10-7395-2013)
43. Agogue H, Brink M, Dinasquet J, Herndl GJ. 2008 Major gradients in putatively nitrifying and non-nitrifying Archaea in the deep North Atlantic. *Nature* **456**, 788–791. (doi:10.1038/nature07535)
44. Sunagawa S *et al.* 2015 Structure and function of the global ocean microbiome. *Science* **348**, 1261359. (doi:10.1126/science.1261359)
45. Rinke C, Chuvpochina M, Mussig AJ, Chaumeil P-A, Davin AA, Waite DW, Whitman WB, Parks DH, Hugenholtz P. 2021 A standardized archaeal taxonomy for the Genome Taxonomy Database. *Nat. Microbiol.* **6**, 946–959. (doi:10.1038/s41564-021-00918-8)
46. Rappé MS, Giovannoni SJ. 2003 The uncultured microbial majority. *Ann. Rev. Microbiol.* **57**, 369–394. (doi:10.1146/annurev.micro.57.030502.090759)
47. Morris RM, Vergin KL, Cho J-C, Rappé MS, Carlson CA, Giovannoni SJ. 2005 Temporal and spatial response of bacterioplankton lineages to annual convective overturn at the Bermuda Atlantic Time-series Study site. *Limnol. Oceanogr.* **50**, 1687–1696. (doi:10.4319/lo.2005.50.5.1687)
48. Letelier RM, Dore JE, Winn CD, Karl DM. 1996 Seasonal and interannual variations in photosynthetic carbon assimilation at Station. *Deep Sea Res. II: Top. Stud. Oceanogr.* **43**, 467–490. (doi:10.1016/0967-0645(96)00006-9)
49. Porschke D. 1997 Macrodipoles unusual electric properties of biological macromolecules. *Biophys. Chem.* **66**, 241–257. (doi:10.1016/S0301-4622(97)00060-4)
50. Lehtovirta-Morley LE, Sayavedra-Soto LA, Gallois N, Schouten S, Stein LY, Prosser JI, Nicol GW. 2016 Identifying potential mechanisms enabling acidophily in the ammonia-oxidizing archaeon '*Candidatus Nitrosotalea devanattera*'. *Appl. Environ. Microbiol.* **82**, 2608–2619. (doi:10.1128/AEM.04031-15)
51. Dupont CL *et al.* 2012 Genomic insights to SAR86, an abundant and uncultivated marine bacterial lineage. *ISME J.* **6**, 1186–1199. (doi:10.1038/ismej.2011.189)
52. Li D-X, Zhang H, Chen X-H, Xie Z-X, Zhang Y, Zhang S-F, Lin L, Chen F, Wang D-Z. 2018 Metaproteomics reveals major microbial players and their metabolic activities during the blooming period of a marine dinoflagellate *Prorocentrum donghaiense*. *Environ. Microbiol.* **20**, 632–644. (doi:10.1111/1462-2920.13986)
53. Müller T, Walter B, Wirtz A, Burkovski A. 2006 Ammonium toxicity in bacteria. *Curr. Microbiol.* **52**, 400–406. (doi:10.1007/s00284-005-0370-x)
54. Lever MA, Rogers KL, Lloyd KG, Overmann J, Schink B, Thauer RK, Hoehler TM, Jørgensen BB. 2015 Life under extreme energy limitation: a synthesis of laboratory- and field-based investigations. *FEMS Microbiol. Rev.* **39**, 688–728. (doi:10.1093/femsre/fuv020)
55. Qin W *et al.* 2020 Alternative strategies of nutrient acquisition and energy conservation map to the biogeography of marine ammonia-oxidizing archaea. *ISME J.* **14**, 2595–2609. (doi:10.1038/s41396-020-0710-7)
56. Walker CB *et al.* 2010 *Nitrosopumilus maritimus* genome reveals unique mechanisms for nitrification and autotrophy in globally distributed marine crenarchaea. *PNAS* **107**, 8818–8823. (doi:10.1073/pnas.0913533107)
57. Santoro AE *et al.* 2015 Genomic and proteomic characterization of '*Candidatus Nitrosopelagicus brevis*': an ammonia-oxidizing archaeon from the open ocean. *PNAS* **112**, 1173–1178. (doi:10.1073/pnas.1416223112)
58. Bèjà O *et al.* 2000 Bacterial rhodopsin: evidence for a new type of phototrophy in the sea. *Science* **289**, 1902–1906. (doi:10.1126/science.289.5486.1902)
59. Sabehi G, Bèjà O, Suzuki MT, Preston CM, DeLong EF. 2004 Different SAR86 subgroups harbour divergent proteorhodopsins. *Environ. Microbiol.* **6**, 903–910. (doi:10.1111/j.1462-2920.2004.00676.x)
60. Sabehi G, Loy A, Jung K-H, Partha R, Spudis JL, Isaacson T, Hirschberg J, Wagner M, Bèjà O. 2005 New insights into metabolic properties of marine bacteria encoding proteorhodopsins. *PLOS Biol.* **3**, e273. (doi:10.1371/journal.pbio.0030273)
61. West NJ, Lepère C, de Manes C-L, Catala P, Scanlan DJ, Lebaron P. 2016 Distinct spatial patterns of SAR11, SAR86, and Actinobacteria diversity along a transect in the ultra-oligotrophic South Pacific Ocean. *Front. Microbiol.* **7**, 234. (doi:10.3389/fmicb.2016.00234)

62. Fiksen Ø, Follows MJ, Aksnes DL. 2013 Trait-based models of nutrient uptake in microbes extend the Michaelis-Menten framework. *Limnol. Oceanogr.* **58**, 193–202. (doi:10.4319/lo.2013.58.1.0193)
63. Collier JL, Baker KM, Bell SL. 2009 Diversity of urea-degrading microorganisms in open-ocean and estuarine planktonic communities. *Environ. Microbiol.* **11**, 3118–3131. (doi:10.1111/j.1462-2920.2009.02016.x)
64. Connelly TL, Baer SE, Cooper JT, Bronk DA, Wawrik B. 2014 Urea uptake and carbon fixation by marine pelagic bacteria and archaea during the arctic summer and winter seasons. *Appl. Environ. Microbiol.* **80**, 6013–6022. (doi:10.1128/AEM.01431-14)
65. Nikrad MP, Cottrell MT, Kirchman DL. 2014 Uptake of dissolved organic carbon by Gammaproteobacterial subgroups in coastal waters of the West Antarctic Peninsula. *Appl. Environ. Microbiol.* **80**, 3362–3368. (doi:10.1128/AEM.00121-14)
66. Delmont TO, Kiefl E, Kilinc O, Esen OC, Uysal I, Rappé MS, Giovannoni S, Eren AM. 2019 Single-amino acid variants reveal evolutionary processes that shape the biogeography of a global SAR11 subclade. *Elife* **8**, e46497. (doi:10.7554/eLife.46497)
67. Noell SE, Giovannoni SJ. 2019 SAR11 bacteria have a high affinity and multifunctional glycine betaine transporter. *Environ. Microbiol.* **21**, 2559–2575. (doi:10.1111/1462-2920.14649)
68. Malmstrom RR, Kiene RP, Cottrell MT, Kirchman DL. 2004 Contribution of SAR11 bacteria to dissolved dimethylsulfoniopropionate and amino acid uptake in the North Atlantic Ocean. *Appl. Environ. Microbiol.* **70**, 4129–4135. (doi:10.1128/AEM.70.7.4129-4135.2004)
69. Giovannoni SJ *et al.* 2005 Genome streamlining in a cosmopolitan oceanic bacterium. *Science* **309**, 1242–1245. (doi:10.1126/science.1114057)
70. Grzymalski JJ, Dussaq AM. 2012 The significance of nitrogen cost minimization in proteomes of marine microorganisms. *ISME J* **6**, 71–80. (doi:10.1038/ismej.2011.72)
71. Inwood WB, Hall JA, Kim K-S, Fong R, Kustu S. 2009 Genetic evidence for an essential oscillation of transmembrane-spanning segment 5 in the *Escherichia coli* ammonium channel AmtB. *Genetics* **183**, 1341–1355. (doi:10.1534/genetics.109.109579)
72. Huergo LF, Chandra G, Merrick M. 2013 PII signal transduction proteins: nitrogen regulation and beyond. *FEMS Microbiol. Rev.* **37**, 251–283. (doi:10.1111/j.1574-6976.2012.00351.x)
73. Buchfink B, Xie C, Huson DH. 2015 Fast and sensitive protein alignment using DIAMOND. *Nat. Methods* **12**, 59–60. (doi:10.1038/nmeth.3176)
74. Bateman A *et al.* 2017 UniProt: the universal protein knowledgebase. *Nucleic Acids Res.* **45**, D158–D169. (doi:10.1093/nar/gkw1099)
75. Abascal F, Zardoya R, Telford MJ. 2010 TranslatorX: multiple alignment of nucleotide sequences guided by amino acid translations. *Nucleic Acids Res.* **38**, W7–W13. (doi:10.1093/nar/gkq291)
76. Fu L, Niu B, Zhu Z, Wu S, Li W. 2012 CD-HIT: accelerated for clustering the next-generation sequencing data. *Bioinformatics* **28**, 3150–3152. (doi:10.1093/bioinformatics/bts565)
77. Milanese A *et al.* 2019 Microbial abundance, activity and population genomic profiling with mOTUs2. *Nat. Commun.* **10**, 1014. (doi:10.1038/s41467-019-08844-4)
78. Wickham H. 2011 ggplot2. *WIREs Comput. Stat.* **3**, 180–185. (doi:10.1002/wics.147)
79. R Core Team. 2020 *R: a language and environment for statistical computing*. Vienna, Austria: R Foundation for Statistical Computing.
80. Katoh K, Standley DM. 2013 MAFFT multiple sequence alignment software version 7: improvements in performance and usability. *Mol. Biol. Evol.* **30**, 772–780. (doi:10.1093/molbev/mst010)
81. Omasits U, Ahrens CH, Müller S, Wollscheid B. 2014 Protter: interactive protein feature visualization and integration with experimental proteomic data. *Bioinformatics* **30**, 884–886. (doi:10.1093/bioinformatics/btt607)
82. Käll L, Krogh A, Sonnhammer ELL. 2007 Advantages of combined transmembrane topology and signal peptide prediction—the Phobius web server. *Nucleic Acids Res.* **35**, W429–W432. (doi:10.1093/nar/gkm256)
83. Bachem. In press. Bachem Peptide Calculator. *Bachem Peptide Calculator*. See <https://www.bachem.com/service-support/peptide-calculator/> (accessed on 12 October 2020).
84. Kellom M, Pagliara S, Richards TA, Santoro AE. 2022 Exaggerated trans-membrane charge of ammonium transporters in nutrient-poor marine environments. Figshare. (doi:10.6084/m9.figshare.c.6070031)